Biologics: Targets and Therapy

Dovepress
Taylor & Francis Group

Open Access Full Text Article

ORIGINAL RESEARCH

Network Pharmacology-Based Exploration: Non-Targeted Metabolites of *Lactobacillus*-Fermented *Chaenomeles speciosa (Sweet) Nakai, Smilax glabra Roxb.* and *Pueraria montana var. Lobata* in Uric Acid Metabolism Intervention

Wei Tan, Zongjun Li

College of Food Science and Technology, Hunan Agricultural University, Changsha, Hunan, People's Republic of China

Correspondence: Zongjun Li, Email hnlizongjun@163.com

Background: Previous studies have demonstrated that numerous medicine and food homology (MFH) possess the potential to regulate purine metabolism disorders, promote uric acid excretion, and alleviate hyperuricemia symptoms. Examples include CS (*Chaenomeles speciosa (Sweet) Nakai*), SR (*Smilax glabra Roxb.*) and PL (*Pueraria montana var. lobata*).

Methods: Metabolomics was employed to analyze the compositional changes in medicinal and edible extracts before and after fermentation. Network pharmacology and molecular docking studies were further utilized to elucidate the interactions between these differential metabolites and the core targets of hyperuricemia. In vitro enzyme activity assays were conducted to confirm the therapeutic effects.

Results: A total of 283, 248, and 18 differential metabolites were identified in CS,SR and PL samples, respectively. Among these, 54 significantly upregulated differential metabolites were selected for screening. Based on these metabolites, 53 HUA-related targets were identified for CS, SR and PL. Functional enrichment analysis revealed their roles in inflammatory stress and uric acid production pathways, particularly the MAPK signaling pathway and purine metabolism regulated by XDH. Additionally, other targets in the purine metabolism pathway, such as ADA, PNP, AMPD3, and IMPDH2, were co-regulated. Enzyme activity assays indicate that fermented MFH more effectively inhibits XOD, thereby regulating the conversion of xanthine and hypoxanthine into uric acid. Molecular docking revealed two significantly upregulated compounds in *CS*; and five in PL; and four in SR. exhibit strong binding to XOD.

Conclusion: These findings provide theoretical support for FMFH as a potential effective component in preventing and treating hyperuricemia. Our research demonstrates that FMFH targets multiple pathways associated with hyperuricemia, offering a promising approach for preventing this condition.

Keywords: MFH, LAB, HUA, UA, network pharmacology, metabonomics

Introduction

Hyperuricemia(HUA) is a disorder of purine metabolism characterized primarily by elevated uric acid levels in the blood. It is diagnosed when levels exceed 420 μmol/L in males and 360 μmol/L in females. The global prevalence of hyperuricemia has now reached 13.3%.[1] Common medications for gout treatment include allopurinol and febuxostat, but long-term use may cause side effects, including severe allergic reactions.[2] Approximately one-fifth of users experience gastrointestinal, hepatic, renal, hematologic, or cutaneous toxicity,[3] thus contraindicating these drugs in patients with hepatic insufficiency or low blood cell counts.[4]

https://doi.org/10.2147/BTT.S578004
Received: 30 October 2025
Accepted: 27 January 2026
Published: 24 February 2026

Numerous traditional Chinese medicines, such as *Smilax glabra Roxb*.[5] *Plantago asiatica L, Coix lacryma-jobi L*.[6] *Gardenia jasminoides J.Ellis, Cichorium intybus L., Lophatherum gracile Brongn*[7] demonstrate efficacy against hyperuricemia.[8] Among these traditional Chinese medicines, *Chaenomeles speciosa (Sweet) Nakai, Smilax glabra Roxb*., and *Pueraria montana var. lobata* possess multiple efficacies including reducing uric acid production, promoting uric acid excretion, and exerting anti-inflammatory effects. This multi-target synergistic action provides a comprehensive approach for treating hyperuricemia, thereby demonstrating unique advantages and broad development prospects in the prevention and treatment research of complex metabolic diseases, particularly hyperuricemia. The botanical plant names mentioned in the text (in italics), including the authoritative names (non-italic), comply with the latest revision in the "Plant List" from MPNS (http://mpns.kew.org).

The fruit of CS (*Chaenomeles speciosa (Sweet) Nakai*) possesses medicinal and food application value and exhibits beneficial pharmacological properties. It is a commonly used traditional Chinese medicine and has been included in the Chinese Pharmacopoeia (Chinese Pharmacopeia Commission, 2020).[9] In traditional Chinese medicine (TCM), CS is referred to as "Chaenomelis Fructus." It can reduce uric acid, creatinine, and blood urea nitrogen levels and promote uric acid excretion.[10]

The dried rhizome of SR (*Smilax glabra Roxb.)* is known in TCM as "Smilacis Glabrae Rhizoma." It can remove toxins, eliminate dampness, and relax joint movements. It primarily contains flavonoids (TFSG) and polysaccharides. Modern research has found that SR can reduce the expression of IL-1β, IL-6, and TNF-α and inhibit the NF-κB signaling pathway, thereby suppressing the production of inflammatory factors.[11] It exhibits anti-inflammatory, analgesic, and antioxidant effects.[5]

Kudzu root is the dried root of *Pueraria montana var. lobata* and is a common medicinal and edible Chinese herbal medicine, mainly produced in Henan, China. It is often used in combination with Scutellaria baicalensis (Baical Skullcap), Coptis chinensis (Coptis), and licorice to treat inflammation.[12] PL (Kudzu root) contains various flavonoids and flavonoid derivatives. In the treatment of hyperuricemia, it inhibits XOD activity,[13] blocks the TLR4/NF-κB pathway, and suppresses the production of IL-1β and TNF-α.[14]

Fermenting MFH with LAB enables the enzymatic systems within these bacteria[15] to decompose macromolecular substances in *Chaenomeles speciosa (Sweet) Nakai, Smilax glabra Roxb*. and *Pueraria montana var. lobata*; this process generates new bioactive components, increases the concentration of effective constituents, and thereby enhances therapeutic efficacy against hyperuricemia. This approach lays the foundation for the present study. The treatment of HUA using MFH primarily functions through three key mechanisms:[2,16] reducing uric acid production by inhibiting key enzymes in purine metabolism; promoting uric acid excretion by regulating uric acid transporter proteins; and alleviating cellular damage by lowering inflammatory factor levels and modulating NLRP3 and NF-κβ inflammatory pathways. Additionally, other studies suggest that MFH may exert therapeutic effects by regulating gut microbiota composition.[17]

The complex composition of MFH, coupled with the transformation of active components into more diverse and intricate compounds through *Lactobacillus* fermentation, poses significant challenges in elucidating their mechanisms of action for treating hyperuricemia. Network pharmacology aids in identifying potential therapeutic pathways for fermented food-medicine substances by constructing "component-target-pathway" networks.[18] Computational methods such as molecular docking enable detailed investigation of binding sites and stability between components and proteins, thereby elucidating the underlying mechanisms of these substances in treating hyperuricemia.

Materials and Methods

Chemicals and Reagents

Water extract (10:1) of *Chaenomeles speciosa (Sweet) Nakai, Smilax glabra Roxb*. and *Pueraria montana var. lobata*, purchased from Shaanxi Guosheng Science, Industry and Trade Co.(Shaanxi, China). XOD assay kit from Nanjing Jiancheng Bio-Research Institute (Nanjing, China); xanthine oxidase (BR grade) from Shanghai Tufeng Biotechnology Co., Ltd. (Shanghai, China); xanthine (≥98%, Shanghai Yuanye Bio); hypoxanthine (≥98%, Mackulin). Methanol (≥99%, Thermo), 2-Chloro-L-phenylalanine (≥98%, Aladdin), Acetonitrile (≥99.9%, Thermo), Formic acid (LC-MS grade, TCI), Ammonium formate (≥99.9%, Sigma).

LAB Fermentation MFH

Take 100g each of CS (*Chaenomeles speciosa (Sweet) Nakai*), SR (*Smilax glabra Roxb.) and* PL(*Pueraria montana var. lobata*) extract powder. Add 200g water to each to prepare an extract solution. Sterilize at 85°C for 15 minutes before inoculation, then cool and set aside.

Strain Activation: Separately take *Lactobacillus plantarum* LK-A01 (screen from raw milk), *Lactobacillus paracasei* LK-A08 (screen from raw milk), and *Lactobacillus rhamnosus* LK-A28 (CCTCC NO: M 20251983, screen from raw milk). Inoculate each strain at 1–2% inoculum rate into MRS liquid medium and incubate at 37°C for 12 hours to obtain respective lactobacillus cultures (1×10^8 CFU/mL). These were sequentially inoculated at 3% (v/v) into CS, SR, and PL extracts, respectively, and fermented at 37°C for 4 days.[19] The fermented samples were dried in a vacuum freeze-dryer, ground into powder, and stored.

Determination of the Effect of Samples on XOD Activity

Following the method in,[20] optimize the colorimetric assay for determining the inhibition rate of samples against XOD. Fermented and unfermented extracts (10 mg/mL) of CS, SR and PL were incubated separately with XOD (0.02 U/mL) at 37°C for 10 min. After incubation, xanthine (0.48 mmol/L) was added, and absorbance was immediately measured at 293 nm using a microplate reader.

Prepare FCS, FSR, FPL and allopurinol solutions at concentrations of 0, 0.5, 1, 2.5, 5 and 10 mg/mL. The activity of XOD at different concentrations was measured by the above method, and the IC50 value was calculated.

The inhibition rate was calculated using the formula:

$$\text{Inhibition rate}\% = \frac{(\Delta\text{A XOD} - \Delta\text{A sample})}{(\Delta\text{A XOD} - \Delta\text{A blank})} \times 100\%$$

In the formula, ΔA represents the absorbance difference over a specific time period.

Allopurinol as the positive control. GraphPad Prism 9.0 was used to calculate statistical significance. All experiments were independently replicated three times.

Non-Targeted Metabolomics Analysis

Sample Preparation

Take 100 μg of dried extract powder, add 600 μL MeOH (Containing 2-Amino-3-(2-chloro-phenyl)-propionic acid (4 ppm), vortex for 30 seconds, then add steel balls and grind for 60 seconds. Sonicate at room temperature for 15 minutes, followed by centrifugation at 12,000 rpm and 4°C for 10 minutes. Remove the supernatant and filter it through a 0.22 μm membrane for LC-MS detection.[21]

LC-MS Analysis

The LC analysis was performed on a Vanquish UHPLC system (Thermo Fisher Scientific, USA) using an ACQUITY UPLC HSS T3 column (2.1×100 mm, 1.8 μm)(Waters, Milford, MA, USA). The column temperature was maintained at 40 °C with a flow rate of 0.3 mL/min and 2 μL, respectively. For LC-ESI (+)-MS analysis, the mobile phases consisted of (B2) 0.1% formic acid in acetonitrile (v/v) and (A2) 0.1% formic acid in water (v/v). Separation was conducted under the following gradient: 0~1 min, 10% B2; 1~5 min, 10%~98% B2; 5~6.5 min, 98% B2; 6.5~6.6 min, 98%~10% B2; 6.6~8 min, 10% B2. For LC-ESI (-)-MS analysis, the analytes was carried out with (B3) acetonitrile and (A3) ammonium formate (5mM). Separation was conducted under the following gradient: 0~1 min, 10% B3; 1~5 min, 10%~98% B3; 5~6.5 min, 98% B3; 6.5~6.6 min, 98%~10% B3; 6.6~8 min, 10% B3 (1).

Metabolites were detected using a Q Exactive™ hybrid quadrupole-Orbitrap mass spectrometer (Thermo Fisher Scientific) equipped with an ESI source Metabolites were detected using a Q Exactive™ hybrid quadrupole-Orbitrap mass spectrometer (Thermo Fisher Scientific) equipped with an ESI ion source operating in both positive and negative modes. Data were acquired in full MS-ddMS^2 mode with the following settings: spray voltage, ±3.50 kV; capillary temperature, 325 °C; full MS scan range, *m/z* 100–1000 at a resolution of 70,000 FWHM; ddMS^2 scans at a resolution of 17,500 FWHM with a normalized collision energy of 30 eV.

Data Processing and Metabolite Identification

Raw data files were processed using Compound Discoverer™ software (version 3.3, Thermo Fisher Scientific) for peak detection, alignment, normalization, and compound identification. Differential metabolites were screened with thresholds of variable importance in projection (VIP) > 1.0 and P-value < 0.05. Metabolites were identified by matching the accurate mass (mass tolerance < 5 ppm) and MS/MS spectra against the Human Metabolome Database (HMDB) and the mzCloud™ library. For confident annotation, only matches with a mzCloud spectral similarity score above 70 were accepted.

Identification of Bioactive Components and Corresponding Targets in CS, SR and PL

Non-targeted metabolomics analysis identified bioactive components and their targets in CS and SR based on data with VIP > 1 and P-value < 0.05.[22] From these, 54 significantly upregulated metabolites were selected for further screening by applying an additional filter of fold-change (FC) > 1.0. The corresponding targets of these bioactive components were then predicted. Similarly, targeted metabolomics detected flavonoid components in PL, revealing bioactive constituents and their targets.[23,24] Phenolic compounds from HPLC analysis were queried in PubChem to generate SDF files, subsequently processed through Swiss Target Prediction (http://www.swisstargetprediction.ch/, accessed on 5 September 2025).

Predicting the Efficacy of CS, SR and PL in Treating HUA

Target genes for "Hyperuricemia" were retrieved via the GeneCards platform.[25] An intersecting network was constructed between the active components of CS, SR and PL and HUA disease-related targets to screen for overlapping targets for subsequent analysis.

Plot the Venn Diagram of Target Intersections

Using the Venny 2.1 (https://bioinfogp.cnb.csic.es/tools/venny/, accessed on 5 September 2025) website, we constructed a target overlap diagram between CS, SR and PL with HUA to identify overlapping targets between these three MFHs and HUA.

PPI Network Constructed from Overlapping Targets

The STRING database (https://cn.string-db.org/, accessed on 5 September 2025) was utilized to analyze protein-protein interactions (PPI).[26] The intersection of CS, SR and PL ingredient targets and HUA disease targets was queried against the STRING database to obtain a TSV file for constructing the PPI network. Cytoscape 3.9.0 software was then employed for further topological analysis, adjusting node size, shape, color, and layout to construct the complete PPI network and elucidate key regulatory proteins.

GO and KEGG Pathway Enrichment Analysis

GO and KEGG pathway enrichment analyses were performed using the Metascape platform, with results visualized through bar plots and categorical diagrams generated via the Weishengxin Cloud Platform (https://www.bioinformatics.com.cn, accessed on 5 September 2025) and Metware Biotechnology (https://www.metwarebio.com, accessed on 5 September 2025). The results visualized on the bioinformatics platform. Statistical significance was observed at $p<0.05$, where a smaller p-value indicates higher enrichment, and a larger count signifies more enriched genes.[27,28] This reflects the roles of CS, SR and PL in biological processes, molecular functions, cellular components, and signaling pathways during HUA treatment.[29]

Molecular Docking Simulation

Crystal structures of XOD (PDB ID: 2ckj) was acquired from the Protein Data Bank (https://www.rcsb.org, accessed on 15 September 2025). The protein was prepared by removing water molecules and co-crystallized ligands, followed by adding hydrogen atoms and assigning CHARMM force field charges using CB-Dock2's built-in function. The three-dimensional structure of the compound originates from Pubchem (https://pubchem.ncbi.nlm.nih.gov/, accessed on 5 September 2025), and were energy-minimized using the MMFF94 force field. The docking grid was automatically

generated by CB-Dock2 (https://cadd.labshare.cn/cb-dock2/php/index.php, accessed on 15 September 2025) to encompass the enzyme's active site. The resulting pose with the highest predicted binding affinity was selected for further analysis and visualized using PyMOL 3.1.0. (Schrödinger, LLC, New York, NY, USA).[30]

Statistical Analysis

Statistical analysis was performed using GraphPad Prism 9.0. Data are expressed as mean ± standard deviation. Each experiment was repeated three times. Statistical comparisons were conducted using t-tests or one-way analysis of variance (ANOVA). Statistical significance was considered at $p < 0.05$, $p < 0.01$, or $p < 0.001$.

Results

Inhibitory Effects of MFH and FMFH on XOD Enzyme Activity

At the same concentration (10 mg/mL), FMFH demonstrated significantly higher inhibition rates against XOD compared to the MFH group (Figure 1A). Among them, FPL (fermented *Pueraria montana var. lobata*) exhibited the strongest inhibitory capacity at 68.89 ± 2.18%; FSR (fermented *Smilax glabra Roxb.)* followed at 59.16 ± 4.36%; while FCS (fermented *Chaenomeles speciosa (Sweet) Nakai*) recorded 41.74 ± 1.71%. Compared to unfermented PL (32.45 ± 3.20%), SR (29.28 ± 4.42%), and CS (19.87 ± 0.94%).

Among the fermented samples (Figure 1B)., FPL had the strongest inhibitory effect on XOD, with an IC50 value of 1.14± 0.028 mg/mL. The IC50 values of FSR, FCS and allopurinol were 3.21± 0.706 mg/mL, 17.66± 9.564 mg/mL and 0.09± 0.003 mg/mL, respectively.

Identification of Major Bioactive Compounds by HPLC-MS

To identify the key bioactive constituents in CS, SR, and PL extracts, targeted analysis was performed based on the UHPLC-Q-TOF-MS data. Through this analysis, 54 significantly upregulated differential metabolites were screened based on thresholds of variable importance in projection (VIP) > 1, P-value < 0.05, and fold change (FC) > 1. Several characteristic compounds among them were unambiguously identified by matching their retention times and accurate mass spectra with those of authentic standards or literature data. The details of these identified compounds, including their retention times (RT) and observed m/z are summarized in Table 1.

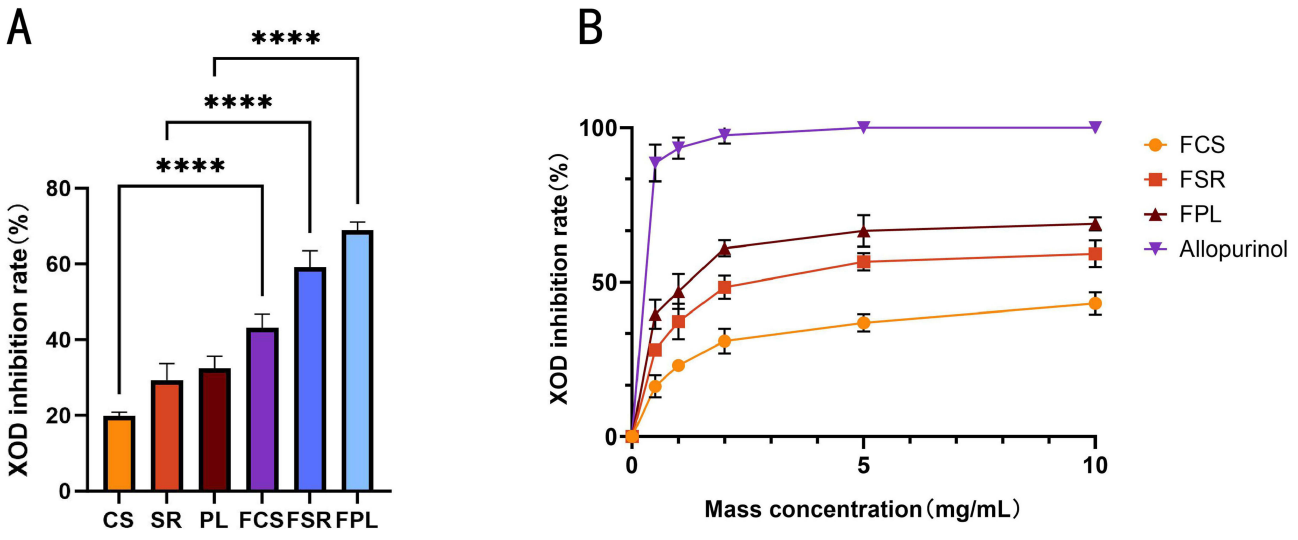

Figure 1 (**A**) Effects of MFH (10 mg/mL) and FMFH (10 mg/mL) on XOD activity ($p<0.05$). (**B**) Inhibitory effect of FCS, FSR, FPL and Allopurinol on XOD activity, n = 3.
Note: **** $P < 0.0001$.
Abbreviations: MFH stands for medicine and food homology; FMFH stands for fermented medicine and food homology; XOD stands for xanthine oxidase; CS stands for *Chaenomeles speciosa (Sweet)*; SR stands for *Smilax glabra Roxb.*; PL stands for *Pueraria montana var. lobate*; FCS stands for fermented *Chaenomeles speciosa (Sweet)*; FSR stands for fermented *Smilax glabra Roxb.*; FPL stands for fermented *Pueraria montana var. lobate*.

https://doi.org/10.2147/BTT.S578004

Table 1 Identification and Characterization of 54 Key Upregulated Metabolites in Fermented MFH Samples

ID	Sample	Compound Name	RT (min)	m/z	Adduct	Formula	Fold Change	P-value	VIP	Identification	Analysis Type
1	CS	1-Hydroxy-2-naphthoic acid	44.80	187.04	[M-H]-	C11H8O3	736.04	8.99E-06	1.62	MS/MS	Non-targeted
2	CS	3′,8-Dimethoxyapigenin 7-glucoside	232.10	493.28	[M+H]+	C23H24O12	251.34	9.76E-04	1.23	MS/MS	Non-targeted
3	CS	Gentisyl alcohol	241.60	141.06	[M+H]+	C7H8O3	148.02	4.36E-07	1.26	MS/MS	Non-targeted
4	CS	Plumbagin	120.00	187.04	[M-H]-	C11H8O3	123.91	1.69E-02	1.57	MS/MS	Non-targeted
5	CS	Fluoranthene	133.80	203.05	[M+H]+	C16H10	113.52	1.69E-02	1.22	MS/MS	Non-targeted
6	CS	Linoleic acid	402.40	263.24	[M-H2O+H]+	C18H32O2	89.46	2.47E-05	1.26	MS/MS	Non-targeted
7	CS	3-Indolecarboxylic acid	201.70	162.06	[M+H]+	C9H7NO2	76.01	2.06E-03	1.26	MS/MS	Non-targeted
8	CS	2-Aminobenzoic acid	197.60	120.08	[M-H2O+H]+	C7H7NO2	68.76	5.26E-04	1.24	MS/MS	Non-targeted
9	CS	Bergapten	133.90	200.05	[M-OH+H]+	C12H8O4	62.82	1.12E-04	1.25	MS/MS	Non-targeted
10	CS	Abscisic Acid	271.80	265.14	[M+H]+	C15H20O4	62.15	1.32E-05	1.26	MS/MS	Non-targeted
11	CS	Argininosuccinic acid disodium	294.10	291.13	[M+H]+	C10H18N4O6	54.09	2.91E-06	1.26	MS/MS	Non-targeted
12	CS	Tryptamine	199.70	144.08	[M-NH3+H]+	C10H12N2	51.69	3.31E-04	1.24	MS/MS	Non-targeted
13	CS	Persicaxanthin	280.10	367.21	[M-H2O+H]+	C25H36O3	50.10	2.44E-04	1.25	MS/MS	Non-targeted
14	CS	Prunasin	50.40	277.07	[M-NH3-H]-	C14H17NO6	44.81	8.20E-05	1.62	MS/MS	Non-targeted
15	CS	9(S)-HPODE	324.70	313.24	[M+H]+	C18H32O4	43.10	1.60E-05	1.26	MS/MS	Non-targeted
16	CS	Prostaglandin E2	362.10	335.22	[M-H2O+H]+	C20H32O5	40.99	1.15E-05	1.26	MS/MS	Non-targeted
17	CS	2-Hydroxybenzyl alcohol	327.10	107.05	[M-H2O+H]+	C7H8O2	29.64	1.98E-03	1.22	MS/MS	Non-targeted
18	CS	Xylitol	54.70	151.06	[M-H]-	C5H12O5	10.12	3.94E-07	1.63	MS/MS	Non-targeted
19	CS	Uracil	123.00	113.03	[M+H]+	C4H4N2O2	3.74	8.94E-03	1.17	MS/MS	Non-targeted
20	CS	Bergaptol	64.40	186.01	[M-NH3+H]+	C11H6O4	2.40	7.60E-04	1.24	MS/MS	Non-targeted
21	CS	Apigenin	376.50	269.22	[M-H]-	C15H10O5	2.12	1.53E-02	1.46	MS/MS	Non-targeted
22	CS	Acacetin	295.70	283.07	[M-H]-	C16H12O5	1.99	2.57E-02	1.41	MS/MS	Non-targeted
23	CS	2-Pentanone	49.40	104.11	[M+NH4]+	C5H10O	1.16	1.92E-02	1.12	MS/MS	Non-targeted
24	SR	Apigenin	298.80	269.05	[M-H]-	C15H10O5	237.65	1.12E-05	1.43	MS/MS	Non-targeted
25	SR	Heneicosylic acid	345.60	325.18	[M-H]-	C21H42O2	175.03	1.33E-04	1.42	MS/MS	Non-targeted
26	SR	Delta-Valerolactone	81.40	101.06	[M+H]+	C5H8O2	135.35	9.42E-07	1.78	MS/MS	Non-targeted
27	SR	Cortisol	327.30	361.24	[M-H]-	C21H30O5	106.39	1.19E-02	1.40	MS/MS	Non-targeted
28	SR	CYCLOHEXANOL	144.00	101.06	[M+H]+	C6H12O	98.52	2.23E-03	1.73	MS/MS	Non-targeted
29	SR	Gentisein	280.9	201.05	[M-CO2+H]+	C13H8O5	75.99	3.04E-06	1.78	MS/MS	Non-targeted
30	SR	Phlorisobutyrophenone	240	219.07	[M+Na]+	C10H12O4	62.12	5.27E-05	1.78	MS/MS	Non-targeted
31	SR	Ginkgolide B	289.5	423.13	[M-H]-	C20H24O10	49.19	4.20E-06	1.43	MS/MS	Non-targeted
32	SR	2-Pentadecanone	262.6	287.22	[M+HCO3]-	C15H30O	44.27	7.25E-07	1.43	MS/MS	Non-targeted
33	SR	Senegalensin	380.5	407.28	[M-H]-	C25H28O5	39.05	5.39E-03	1.42	MS/MS	Non-targeted
34	SR	Hesperetin	299.9	301.07	[M-H]-	C16H14O6	38.61	5.07E-03	1.35	MS/MS	Non-targeted

https://doi.org/10.2147/BTT.S578004

35	SR	Butein	296.5	271.06	[M-H]-	C15H12O5	37.95	1.22E-05	1.43	MS/MS	Non-targeted
36	SR	Lignans	272.2	475.13	[M+HCO3]-	C22H22O8	37.27	8.97E-04	1.4	MS/MS	Non-targeted
37	SR	Coniferaldehyde	333.4	239.06	[M+HCO3]-	C10H10O3	34.26	1.24E-05	1.43	MS/MS	Non-targeted
38	SR	3-HODE + 9-HODE	369.2	295.23	[M-H]-	C18H32O3	15.05	4.86E-08	1.43	MS/MS	Non-targeted
39	SR	4-(4-Hydroxyphenyl)-2-butanone	267.2	147.08	[M-H2O+H]+	C10H12O2	6.76	4.08E-05	1.78	MS/MS	Non-targeted
40	SR	Acetophenone	230.7	121.07	[M+H]+	C8H8O	6.14	6.93E-05	1.77	MS/MS	Non-targeted
41	SR	Benzaldehyde	69.9	124.08	[M+NH4]+	C7H6O	4.77	6.38E-03	1.67	MS/MS	Non-targeted
42	SR	5-Hydroxymethyl-2-furancarboxaldehyde	208	127.04	[M+H]+	C6H6O3	4.23	1.13E-02	1.64	MS/MS	Non-targeted
43	SR	Astragalin	251.1	447.09	[M-H]-	C21H20O11	3.87	4.31E-04	1.41	MS/MS	Non-targeted
44	SR	Multifidol	258.8	193.09	[M-H2O+H]+	C11H14O4	3.73	4.67E-04	1.76	MS/MS	Non-targeted
45	SR	Eugenol	266.1	165.09	[M+H]+	C10H12O2	3.69	2.18E-02	1.57	MS/MS	Non-targeted
46	SR	Pyrocoll	279.6	187.08	[M+H]+	C10H6N2O2	3.65	1.73E-03	1.73	MS/MS	Non-targeted
47	SR	Puerarin	216	417.12	[M+H]+	C21H20O9	2.67	3.71E-03	1.69	MS/MS	Non-targeted
48	SR	Citropten	236.3	189.05	[M-H2O+H]+	C11H10O4	2.09	2.28E-03	1.72	MS/MS	Non-targeted
49	SR	Carbendazim	77.6	192.14	[M+H]+	C9H9N3O2	1.61	7.32E-03	1.66	MS/MS	Non-targeted
50	PL	Biochanin A	19.37	19.37	[M+H]+	C16H12O5	2	1.23E-06	1.16	Standard	Targeted
51	PL	Genistein	16.67	16.67	[M+H]+	C15H10O5	1.88	3.73E-06	1.15	Standard	Targeted
52	PL	Rutin	8.65	8.65	[M+H]+	C27H30O16	1.73	2.06E-03	1.11	Standard	Targeted
53	PL	Genistin	9.75	9.75	[M+H]+	C21H20O10	1.62	1.08E-03	1.12	Standard	Targeted
54	PL	Formononetin	18.47	18.47	[M+H]+	C16H12O4	1.43	5.46E-04	1.13	Standard	Targeted

Abbreviations: RT, retention time; VIP, variable importance in projection; FC, fold change (fermented vs non-fermented); CS stands for *Chaenomeles speciosa (Sweet)*; SR stands for *Smilax glabra Roxb.*; PL stands for *Pueraria montana var. lobate*.

https://doi.org/10.2147/BTT.S578004

Positive and Negative Ion Spectra and Multivariate Statistical Analysis

To elucidate the enhanced efficacy of FMFH compared to MFH extracts, we employed a non-targeted metabolomics approach based on UHPLC-Q-TOF-MS to characterize its chemical profile. Total ion chromatograms (TICs) of CS and SR, shown in Figure 2A–D, provide comprehensive chemical fingerprint profiles: M13 represents the *Chaenomeles speciosa (Sweet) Nakai* group, M46 represents the fermented *Chaenomeles speciosa (Sweet) Nakai* group; T13 represents the *Smilax glabra Roxb*. group, T46 represents the fermented *Smilax glabra Roxb*. group. Total ion chromatograms (TICs) in both positive and negative ion modes demonstrated excellent signal stability across duplicate analyses. Overlapping metabolite TIC curves confirmed consistent retention times and peak intensities.

Principal component analysis (PCA) of the metabolome revealed distinct clustering patterns for *Chaenomeles speciosa (Sweet) Nakai, Smilax glabra Roxb*. and *Pueraria montana var. lobata* revealed distinct clustering patterns ($R^2X = 0.885$; Figure 3A and B), indicating significant metabolic differences between groups. Orthogonal Partial Least Squares Discriminant Analysis (OPLS-DA) was applied to address potential limitations in low-correlation variable detection. G13 represents the *Pueraria montana var. lobata* group, and G79 represents the fermented *Pueraria montana var. lobata* group.

The OPLS-DA score plot revealed distinct separation between M13 and M46 (R2X = 0.73, R2Y = 1, Q2 = 0.98; Figure 3C), between T13 and T46 (R2X = 0.654, R2Y = 1, Q2 = 0.95; Figure 3D), and between G13 and G79 (R2X = 0.975, R2Y = 1, Q2 = 0.99; Figure 3E). Here, R2X and R2Y denote the explained variance in the X (metabolite) and Y (group) matrices, respectively, while Q2 reflects prediction accuracy—values close to 1.0 indicate model stability and reliable predictions.

The OPLS-DA score plots (Figure 3F–H) for CS, SR, and PL demonstrate robust separation between groups, corroborating the PCA results and validating fermentation as a key factor driving distinct metabolic profiles.

Analysis of Differentially Abundant Metabolites in FMFH

The hierarchical clustering heatmaps of FMFH metabolites (Figure 4A–C) reveal significant compositional differences in MFH before and after LAB fermentation. To characterize the major chemical constituents of FCS and FSR, quantitative assessments were conducted for total polysaccharides, total polyphenols, total flavonoids, terpenoids, alkaloids, and other compounds.[31,32] Among these components, the content of total flavonoids was significantly higher (Figure 4D and E), suggesting their potential contribution to the therapeutic efficacy of FMFH. Enrichment bubble plots revealed these metabolites primarily participated in the biosynthesis pathways of flavones and flavanols, as well as isoflavone (Figure 4F and G).

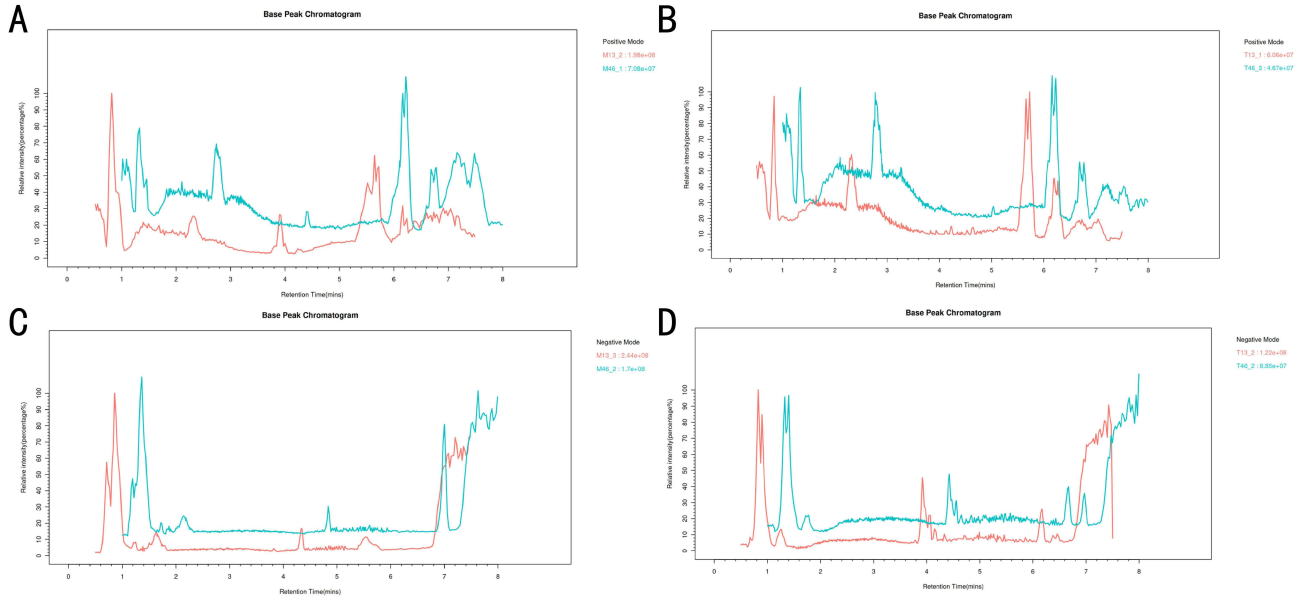

Figure 2 Base peak chromatograms (BPC) of non-targeted metabolomics analysis. (**A**) BPC of *Chaenomeles speciosa (Sweet)* in positive ion mode; (**B**) BPC of *Chaenomeles speciosa (Sweet)* in negative ion mode; (**C**) BPC of *Smilax glabra Roxb*. in positive ion mode; (**D**) BPC of *Smilax glabra Roxb*. in negative ion mode.

https://doi.org/10.2147/BTT.S578004

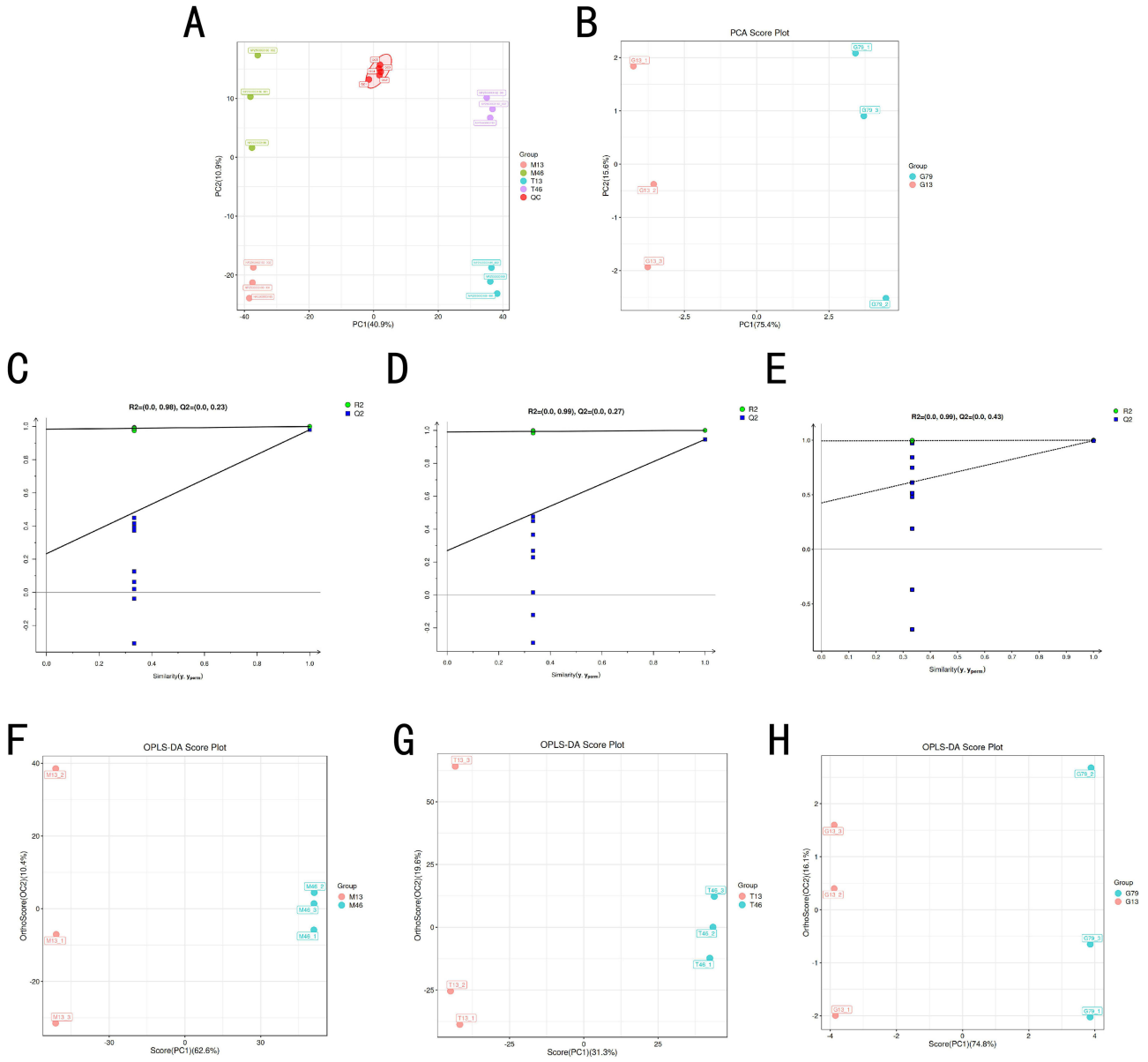

Figure 3 Multivariate statistical analysis of LC-MS data in positive/negative ion modes. (**A**) Principal Component Analysis (PCA) scoreplot for *Chaenomeles speciosa (Sweet)* and *Smilax glabra Roxb*.; (**B**) PCA scoreplot for *Pueraria montana var. lobate*; (**C**) Permutation test validating the OPLS-DA model for *Chaenomeles speciosa (Sweet)*; (**D**) Permutation test validating the OPLS-DA model for *Smilax glabra Roxb*.; (**E**) Permutation test validating the OPLS-DA model for *Pueraria montana var. lobata*.; (**F**) Partial Least Squares Discriminant Analysis (PLS-DA) score plot for *Chaenomeles speciosa (Sweet)*; (**G**) PLS-DA score plot for *Smilax glabra Roxb*.; (**H**) PLS-DA score plot for *Pueraria montana var. lobata*.

Abbreviations: FCS stands for fermented *Chaenomeles speciosa (Sweet)*; FSR stands for fermented *Smilax glabra Roxb*.; FPL stands for fermented *Pueraria montana var.lobate*. M13 represents the *Chaenomeles speciosa (Sweet) Nakai* group, M46 represents the fermented *Chaenomeles speciosa (Sweet) Nakai* group; T13 represents the *Smilax glabra Roxb*. group, T46 represents the fermented *Smilax glabra Roxb*. group.

Collectively, these pathways promote the production of key urate-lowering agents, including 3′,8-Dimethoxyapigenin 7-glucoside and Bergapten in CS, and Apigenin and Butein in SR. (Figure 4F and G), collectively promoting the production of key urate-lowering agents, including 3′,8-Dimethoxyapigenin 7-glucoside and Bergapten in FCS; Apigenin, Butein, Astragalin and Citropten in FSR; and Biochanin A, Genistein, Rutin,[33] Genistin, Formononetin and Daidzein in FPL.

To investigate the potential roles of the significantly upregulated metabolites in uric acid metabolism, we focused on several representative compounds identified in FMFH. Figure 5 displays the chemical structures of these key metabolites. Among them, Bergapten is a furanocoumarin present in FCS, which has been reported in the literature to possess

https://doi.org/10.2147/BTT.S578004

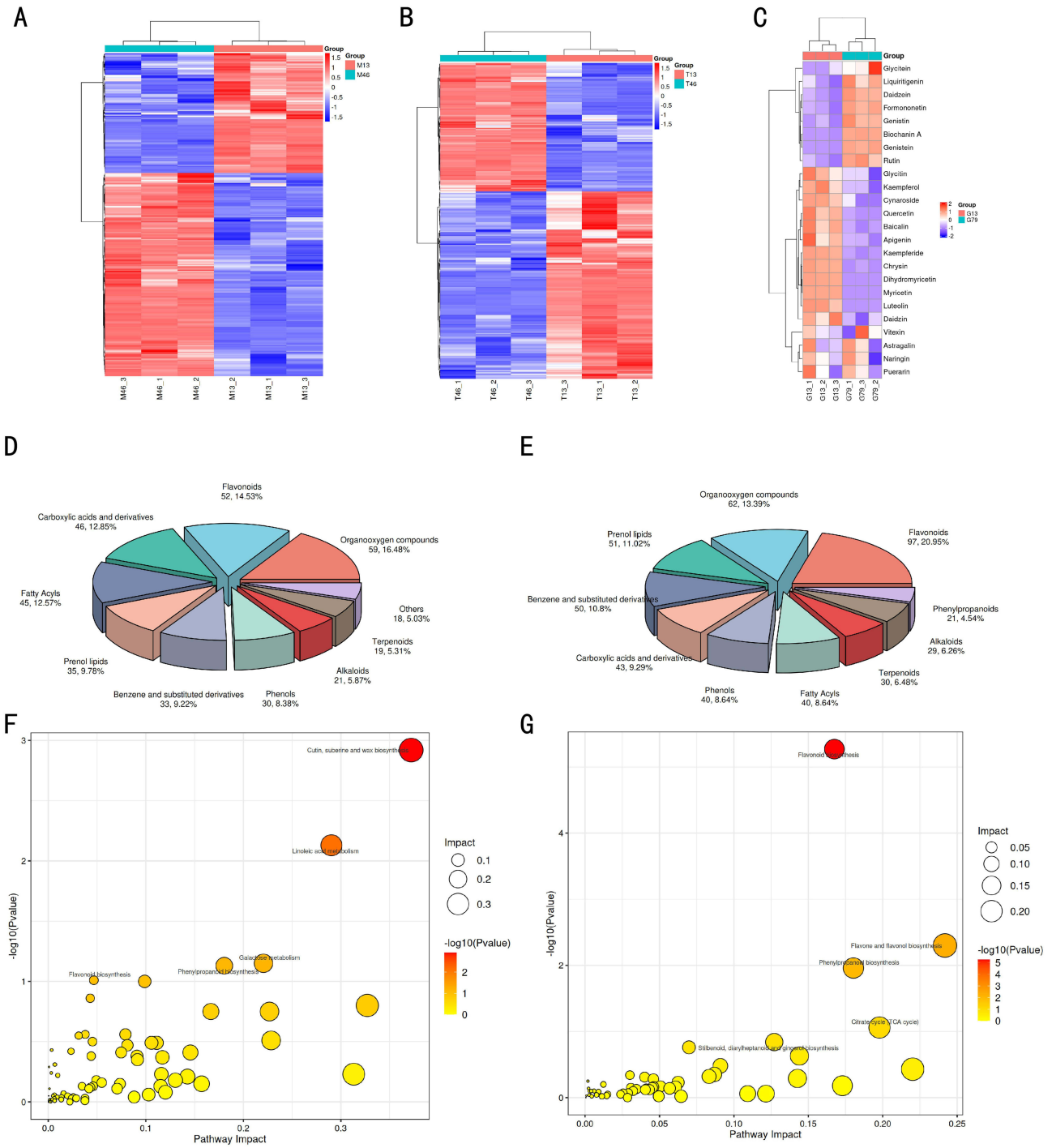

Figure 4 (**A**) Hierarchical clustering heatmap of metabolites from fermented *Chaenomeles speciosa (Sweet)* (log2FC > 1, p < 0.05); (**B**) Hierarchical clustering heatmap of metabolites from fermented *Smilax glabra Roxb.* (log2FC > 1, p < 0.05); (**C**) Hierarchical clustering heatmap of metabolites from fermented *Pueraria montana var.lobate.* (log2FC>1, p<0.05); (**D**) Chemical classification of identified metabolites in *Chaenomeles speciosa (Sweet) Nakai*; (**E**) Chemical classification of identified metabolites in *Smilax glabra Roxb.*; (**F**) Enrichment bubble plot of *Chaenomeles speciosa (Sweet) Nakai* metabolites; (**G**) Enrichment bubble plot of metabolites from *Smilax glabra Roxb.*
Abbreviations: M13 represents the *Chaenomeles speciosa (Sweet) Nakai* group, M46 represents the fermented *Chaenomeles speciosa (Sweet) Nakai* group; T13 represents the *Smilax glabra Roxb.* group, T46 represents the fermented *Smilax glabra Roxb.* group. G13 represents the *Pueraria montana var.lobate* group; G79 represents the fermented *Pueraria montana var.lobate* group.

hepatoprotective activity. Given that the liver is the central organ for purine metabolism and uric acid production, this compound may indirectly regulate uric acid levels by maintaining hepatic metabolic homeostasis. Apigenin, a flavonoid whose content increased significantly in FSR, has been confirmed by multiple studies to exhibit anti-inflammatory and

https://doi.org/10.2147/BTT.S578004

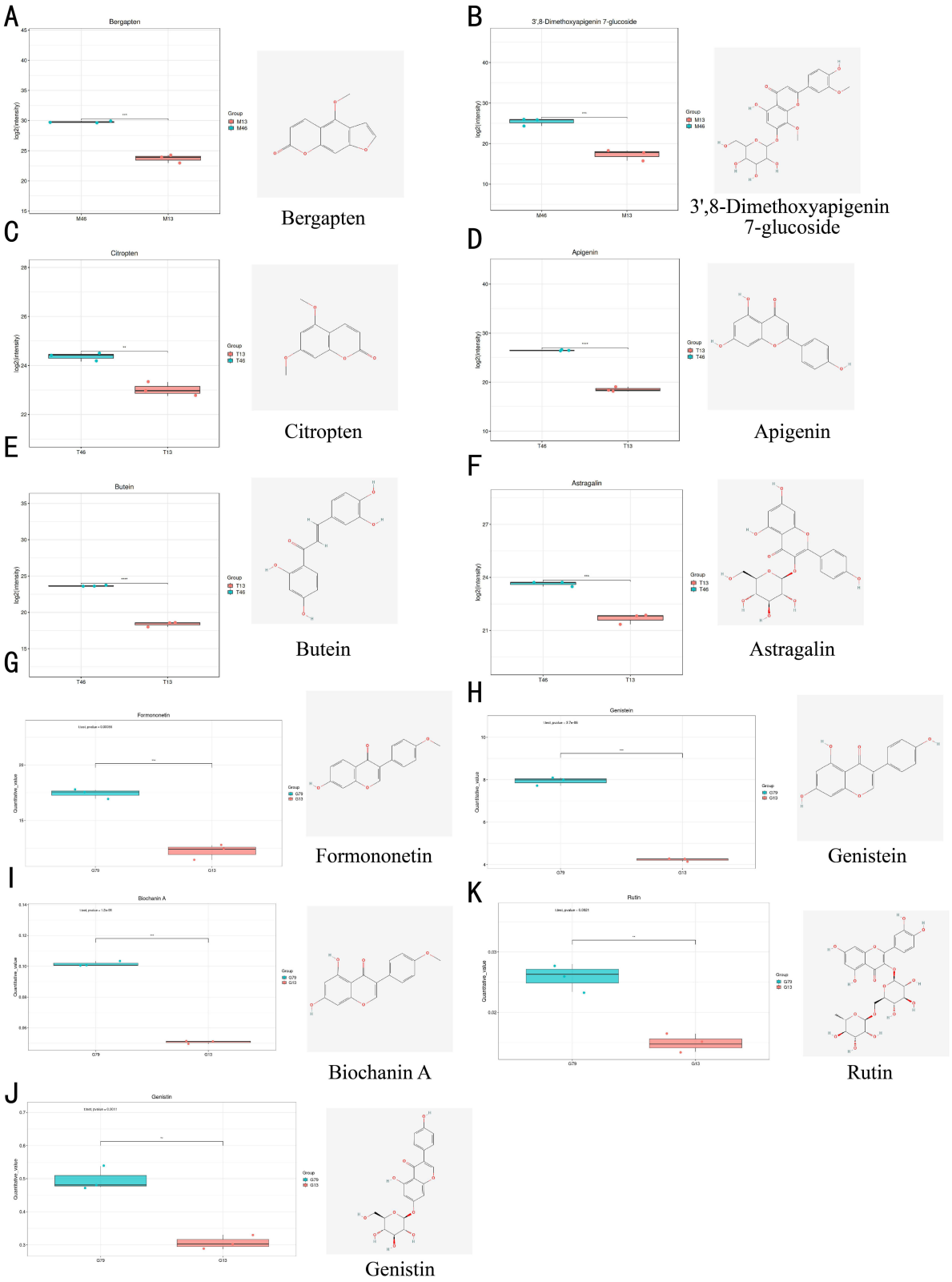

Figure 5 Box distribution map of 11 differentially expressed metabolites. (**A**) Bergapten; (**B**) 3′,8-Dimethoxyapigenin 7-glucoside; (**C**) Citropten; (**D**) Apigenin; (**E**) Butein; (**F**) Astragalin; (**G**) Formononetin; (**H**) Genistein; (**I**) Biochanin A; (**J**) Genistin; (**K**) Rutin. The horizontal axis represents different groups, and the vertical axis represents the range of quantitative values of metabolites. Intergroup stars indicate the significance of the difference between the two groups, ** P < 0.01, *** P < 0.001, **** P < 0.0001.

https://doi.org/10.2147/BTT.S578004

antioxidant properties, potentially helping to alleviate the oxidative stress and inflammatory damage associated with hyperuricemia. Genistein, the major isoflavone in FPL, is a known phytoestrogen and signaling pathway modulator that may intervene in the metabolic disorders related to hyperuricemia through multiple pathways.

Screening and Identification of Active Components and Their Corresponding Targets in MFH and construction of the "Compound-Target" Network

Combining metabolomics data, 691 target predictions for 54 candidate compounds were retrieved using TCMSP, Phar mapper and Swiss target Prediction databases. A "candidate compound-target" network was constructed, and node degree values were calculated in Cytoscape 3.10.3 (Figure 6A). Higher values indicate stronger correlations.

PPI Network Construction

To elucidate how these components exert effects, a network pharmacology analysis was conducted. After comparing differential metabolites-targets with HUA targets, 53 overlapping targets were identified (Figure 6A), suggesting their potential involvement in MFH's anti-hyperuricemic action. Uploading these 53 targets to the STRING database enabled the construction of a protein-protein interaction (PPI) network (Figure 6B). Node degree values were calculated in Cytoscape 3.10.3 (Figure 6C). The top 12 ranked targets:IL6, TNF, PPARG, XDH, ACE, SIRT1, MAOA, G6PD, PTGS2, PARP1, ABCG2, and ADA, emerged as potential key targets (Figure 6D) significantly influenced by HUA. Among these, XDH (xanthine oxidase) and ADA (adenosine deaminase), along with lower-ranked but still regulated enzymes PNP (purine nucleoside phosphorylase), AMPD3 (adenosine monophosphate deaminase 3), and IMPDH2 (inosine monophosphate dehydrogenase 2), all participate in purine metabolism pathways primarily occurring in the liver.

GO and KEGG Pathway Analysis

To elucidate the biological relevance of these targets, GO and KEGG pathway enrichment analyses were performed. The top 10 GO terms and top 20 KEGG pathways are shown in Figure 6E and F, respectively. In this study, Gene Ontology (GO) analysis of the 53 compound targets indicated their potential involvement in purine metabolism, compound metabolism processes, AMPK signaling pathway regulation, and NF-κB signaling pathway (Figure 6F). Notably, purine metabolism and MAPK signaling emerged as key pathways implicated in HUA pathogenesis, with XDH, IL6, and TNF identified as central regulatory nodes.[34] Notably, purine metabolism pathways and the MAPK signaling pathway emerged as key mechanisms implicated in the pathogenesis of HUA, with XDH, IL6, and TNF identified as central regulatory nodes.

Protein-Compound Docking Simulation

The shared core targets XDH, IL6, and TNF were identified through network pharmacology analysis. Considering XOD as the key enzyme regulating uric acid production, XOD was used as the representative structure for molecular docking.

To identify potential XOD inhibitors from the differentially upregulated metabolites, we employed a multi-step selection strategy: (1) Primary screening for significance: Metabolites were first filtered to ensure significant upregulation after fermentation based on thresholds of VIP > 1, P-value < 0.01, and $Log_2FC > 0.5$. (2) Priority screening based on biological relevance: From the pool of 54 upregulated metabolites, we prioritized compounds belonging to structural classes (eg, flavonoids, coumarins) with documented evidence of XOD inhibitory activity in existing literature. (3) Computational validation of binding: The prioritized compounds were then subjected to molecular docking against XOD. The final selection of eleven compounds was based on their superior predicted binding affinities, representing the most promising candidates from this computational validation step. Consequently, two, four, and five differential metabolites were selected from CS, SR, and PL, respectively (Table 2).

Figure 5A–K shows the box-type distribution map of these 11 metabolites. Each of the 11 compounds was docked against XOD to validate interactions between the compounds and the target protein. Generally, lower binding energy indicates more stable ligand-receptor interactions, with docking scores ≤-5 kcal/mol suggesting stable interactions between molecules. The binding energies of the 11 FMFH metabolites (Table 2) ranged from −6.7 to −10.7 kcal/mol,

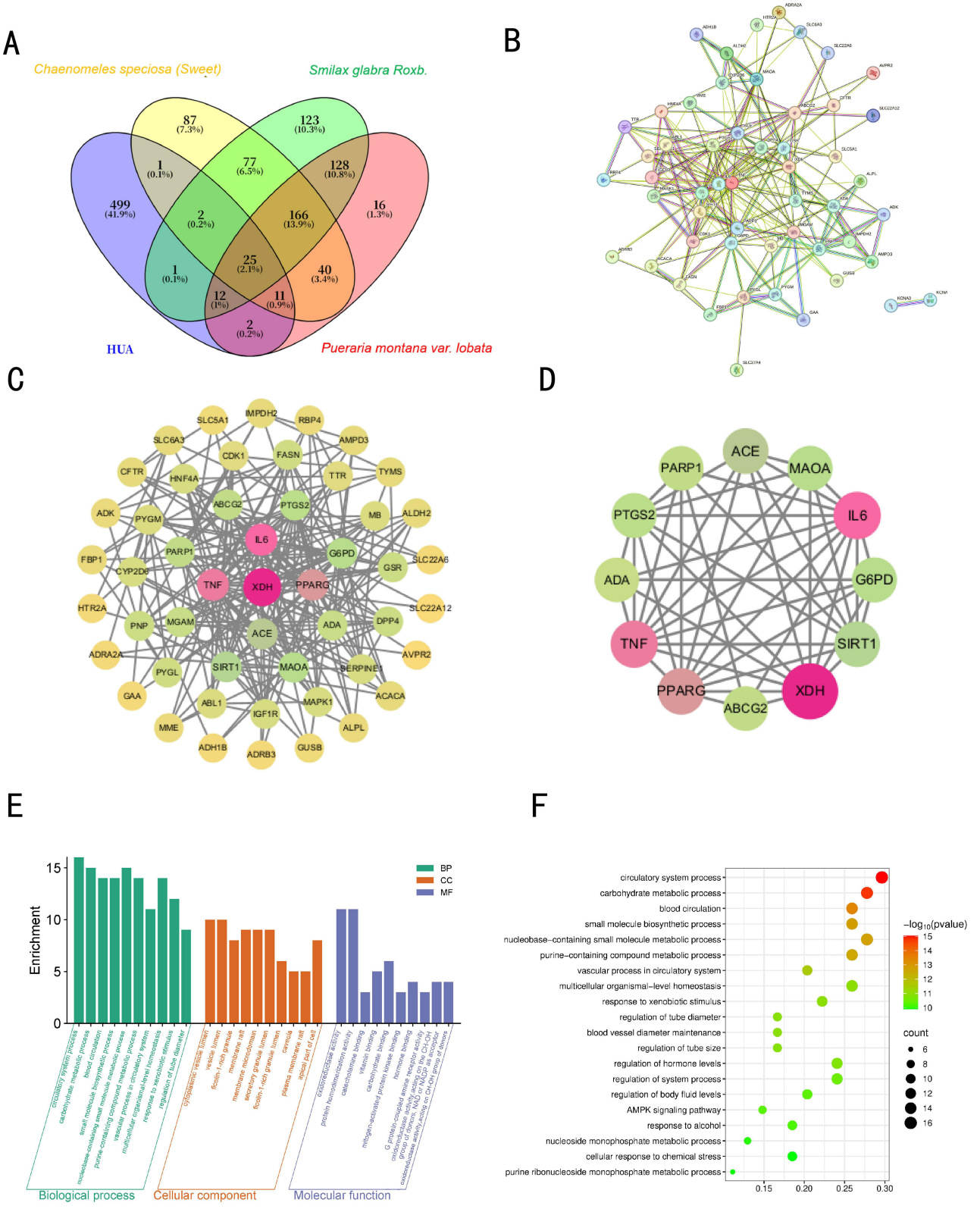

Figure 6 GO and KEGG enrichment analysis. (**A**) The Venn diagram shown the overlapping genes of HUA and MFH. (**B**) Construction and analysis of an interactive protein-protein interaction (PPI) network based on the STRING database, involving 53 MFH compounds targeting HUA. (**C**) Impact of MFH compounds on the protein-protein interaction (PPI) network targeting HUA. Nodes represent distinct proteins. Edges denote protein-protein associations; circle size indicates the strength of data support. (**D**) Protein interaction network of the top 12 proteins by degree. (**E**) GO enrichment analysis revealing the BP, CC, and MF functional attributes of MFH against HUA. (**F**)KEGG pathway analysis.

https://doi.org/10.2147/BTT.S578004

Table 2 11 Compounds with Potential Interference Effects on Purine Metabolism

ID	Sample	Compounds	Class	Formula	Log2FC	-Log10 (P.value)	FDR	VIP	Affinity (kcal/mol)
1	CS	Bergapten	Coumarins and derivatives	C12H8O4	5.97	3.95	0.001173	1.253082	−6.9
2	CS	3′,8-Dimethoxyapigenin 7-glucoside	Flavonoids	C23H24O12	7.97	3.01	0.004658	1.231728	−10.3
3	SR	Citropten	Coumarins and derivatives	C11H10O4	1.33	2.64	0.046208	1.720189	−6.7
4	SR	Apigenin	Flavonoids	C30H30O19	7.89	4.95	0.000568	1.427891	−8.3
5	SR	Butein	Flavonoids	C15H12O5	5.25	4.91	0.000577	1.426606	−8.8
6	SR	Astragalin	Flavonoids	C21H20O11	1.95	3.37	0.004329	1.40684	−9.6
7	PL	Formononetin	Flavonoids	C16H12O4	0.51	3.26	0.001817	1.134566	−8.3
8	PL	Genistein	Flavonoids	C15H10O5	0.91	5.43	4.47E-05	1.154537	−8.3
9	PL	Biochanin A	Flavonoids	C16H12O5	1.00	5.91	2.96E-05	1.155179	−8.3
10	PL	Genistin	Flavonoids	C21H20O10	0.70	2.97	0.0028	1.124713	−9.7
11	PL	Rutin	Flavonoids	C27H30O16	0.79	2.69	0.004491	1.113337	−10.7

Abbreviations: VIP, Variable Importance in Projection; FDR, False Discovery Rate; Log2FC, log_2 (Fold Change). CS stands for *Chaenomeles speciosa (Sweet)*; SR stands for *Smilax glabra Roxb*.; PL stands for *Pueraria montana var. lobate*.

with most metabolites exhibiting binding energies around −8.3 kcal/mol, indicating strong binding affinity to XOD. Compounds from FCS appear white (Figure 7A and B), those from FSR yellow (Figure 7C–F), and those from FPL blue (Figure 7G–K). These 11 compounds bind to distinct amino acid residues on xanthine oxidase, providing theoretical support for enzyme activity experiments.

Discussion

HUA is a metabolic disorder characterized by diverse and complex etiologies and complications. Most patients suffer from pain, and the disease severely impacts their quality of life. Drugs targeting uric acid production inhibition and excretion promotion to reduce uric acid levels are associated with varying degrees of side effects, highlighting the urgent need for novel therapeutic approaches. Research indicates that MFH[35,36] can alleviate HUA through multiple pathways, and long-term use can maintain uric acid levels within a healthy range, creating considerable therapeutic interest for treating gout.[18]

Although significant research progress has been made regarding MFH in the field of gout,[37] the complex composition of MFH still hinders our exploration of its specific role and therapeutic mechanisms in preventing and treating HUA to some extent.[38] Therefore, this study aims to integrate network pharmacology and metabolomics to investigate the mechanisms and molecular targets of *Chaenomeles speciosa (Sweet) Nakai, Smilax glabra Roxb*. and *Pueraria montana var. lobata* in HUA. Concurrently, LAB fermentation is employed to decompose large macromolecular compounds in MFH that are difficult for the human body to absorb, thereby increasing the content of active substances and enhancing MFH's ability to inhibit uric acid production. This approach provides new insights for the comprehensive treatment of HUA.

This study employed integrated research methods including metabolomics, network pharmacology, and molecular docking to identify 549 differentially expressed metabolites in FMFH. Based on significantly up-regulated values before and after fermentation, 53 potential targets were selected for network pharmacology analysis. With MFH polysaccharides and flavonoids as key active components, the top 12 targets most affected by MFH were identified through protein-protein interaction (PPI) analysis: IL6, TNF, PPARG, XDH, ACE, SIRT1, MAOA, G6PD, PTGS2, PARP1, ABCG2, and ADA. Multiple compound metabolic pathways (flavonoid metabolism/isoflavone metabolism) were closely associated with KEGG-enriched pathways, including purine metabolism and MAPK signaling pathways. Results from in vitro enzyme activity assays further validate that LAB-fermented MFH may regulate purine metabolism by inhibiting XOD, ADA, and PNP, while network predictions suggest it may also promote uric acid excretion via transporters like ABCG2.

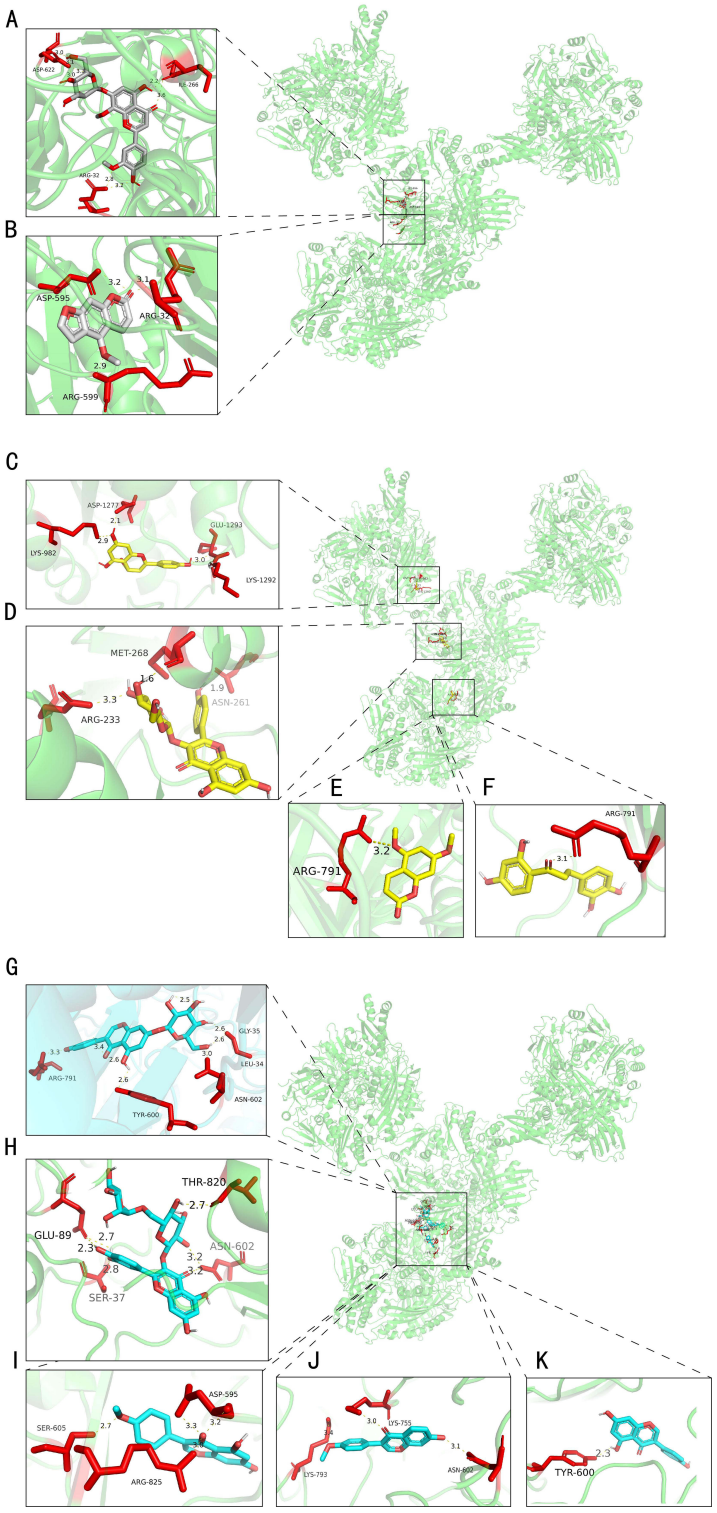

Figure 7 Molecular docking. Molecular docking analysis of key upregulated metabolites with xanthine oxidase (XOD). (**A**) Interaction between bergapten (from FCS) and the XOD active site; (**B**) Interaction between 3′,8-dimethoxyapigenin 7-glucoside (from FCS) and the XOD active site; (**C**) Interaction between apigenin (from FSR) and the XOD active site; (**D**) Interaction between astragalin (from FSR) and the XOD active site; (**E**) Interaction between butein (from FSR) and the XOD active site; (**F**) Interaction between citropten (from FSR) and the XOD active site; (**G**) Interaction between biochanin A (from FPL) and the XOD active site; (**H**) Interaction between genistein (from FPL) and the XOD active site; (**I**) Interaction between genistin (from FPL) and the XOD active site; (**J**) Interaction between rutin (from FPL) and the XOD active site; (**K**) Interaction between formononetin (from FPL) and the XOD active site. White represents metabolites from fermented *Chaenomeles speciosa (Sweet)*, yellow represents metabolites from fermented *Smilax glabra Roxb*., blue represents metabolites from fermented *Pueraria Montana var. lobate*., and red indicates amino acid residues interacting with the metabolites.

Abbreviation: XOD stands for xanthine oxidase.

https://doi.org/10.2147/BTT.S578004

The efficacy of FMFH likely stems from the synergistic actions of its diverse bioactive components, rather than a single compound. Metabolomics revealed upregulated flavonoids (eg, apigenin, genistein) and phenolic acids, each with distinct but complementary pharmacological profiles. For instance, certain flavonoids may directly inhibit XOD activity, while others (like astilbin) mitigate inflammation by downregulating IL-6 and TNF-α via the MAPK pathway. Simultaneously, other components may upregulate the efflux transporter ABCG2 to enhance renal and intestinal uric acid excretion. This multi-target, multi-pathway synergy mirrors the holistic principle of herbal medicine and may offer a superior therapeutic advantage by addressing the complex network of HUA pathogenesis—simultaneously reducing production, alleviating inflammation, and promoting excretion—potentially with fewer side effects compared to single-target drugs.

Purine metabolism in the liver is the primary source of uric acid, with XOD serving as the key terminal enzyme and a major therapeutic target.[39,40] Our in vitro assays confirmed that fermentation significantly enhanced MFH's ability to inhibit XOD activity.[41,42] Beyond production, UA homeostasis depends on excretion transporters such as ABCG2, a crucial target for promoting UA clearance.[43,44]

Metabolomics revealed that fermentation led to the marked upregulation of multiple flavonoid compounds across FCS, FSR, and FPL extracts. Notably, components like astilbin from SR and various isoflavones from PL have been independently reported to possess anti-inflammatory properties, such as inhibiting the MAPK pathway[45] and down-regulating pro-inflammatory cytokines like IL-6 and TNF-α.[46] Importantly, molecular docking suggested that many of these upregulated compounds can directly bind to and inhibit XOD.

This study employed LC/MS metabolomics to reveal significant compositional alterations in FMFH. Metabolomic analysis indicated varying degrees of upregulation in key therapeutic compounds for HUA within FCS, FSR and FPL, such as p-coumaroyl from FCS, which may be converted into bergapten and 3′,8-dimethoxyapigenin-7-glucoside via the flavonoid biosynthetic pathway during LAB fermentation. Apigenin, astragalin, butein, and citropten in FSR similarly accumulated through this pathway. In FPL, the classical flavonoid synthesis pathway is inhibited while the isoflavone metabolic pathway is activated, leading to the accumulation of biochanin A, genistein, genistin, rutin, and formononetin during the reaction. All 11 compounds can bind to XOD, inhibiting purine metabolism reactions and thereby affecting UA levels in HUA patients. This finding aligns with in vitro experiments on XOD activity.

This sets the stage for a coordinated therapeutic strategy. The efficacy of FMFH likely stems not from a single compound, but from the synergistic actions of its diverse bioactive components. For instance, while some flavonoids directly inhibit XOD to reduce UA production, others (like astilbin) may concurrently mitigate HUA-related inflammation by downregulating IL-6 and TNF-α. Simultaneously, other components could enhance UA excretion via transporters like ABCG2. This multi-target, multi-pathway synergy mirrors the holistic principle of herbal medicine, potentially offering a superior therapeutic advantage by addressing the complex network of HUA pathogenesis with fewer side effects compared to single-target drugs.

In addition, the association between *Lactobacillus* and purine metabolism has been extensively studied in gout treatment.[47] It has been reported that LAB can alleviate allergic reactions and reduce serum cholesterol levels; they can also decrease uric acid (UA) production and accumulation. In mouse experiments,[48] *Lactobacillus plantarum* intervention significantly improved disease symptoms in HUA mice, demonstrating favorable therapeutic effects. Metabolites from kidney disease induce alterations in gut microbiota, while probiotic supplementation modifies the structure and composition of the intestinal microbiome in HUA patients. Probiotics suppress inflammation by reshaping the gut microbiota.

In conclusion, based on our integrated analysis, we propose a working model (Figure 8) in which FMFH may alleviate HUA potentially through preventing and treating hyperuricemia by influencing targets across uric acid production, inflammation, and excretion pathways. The fermentation process significantly enhances this multi-target potential. It is important to acknowledge that the current mechanistic insights are predictive, relying on omics and computational analyses without in vivo pharmacological confirmation. Consequently, validating the preventive and therapeutic effects of FMFH, along with its underlying mechanisms, in relevant animal models constitutes an essential future direction to substantiate our working model.

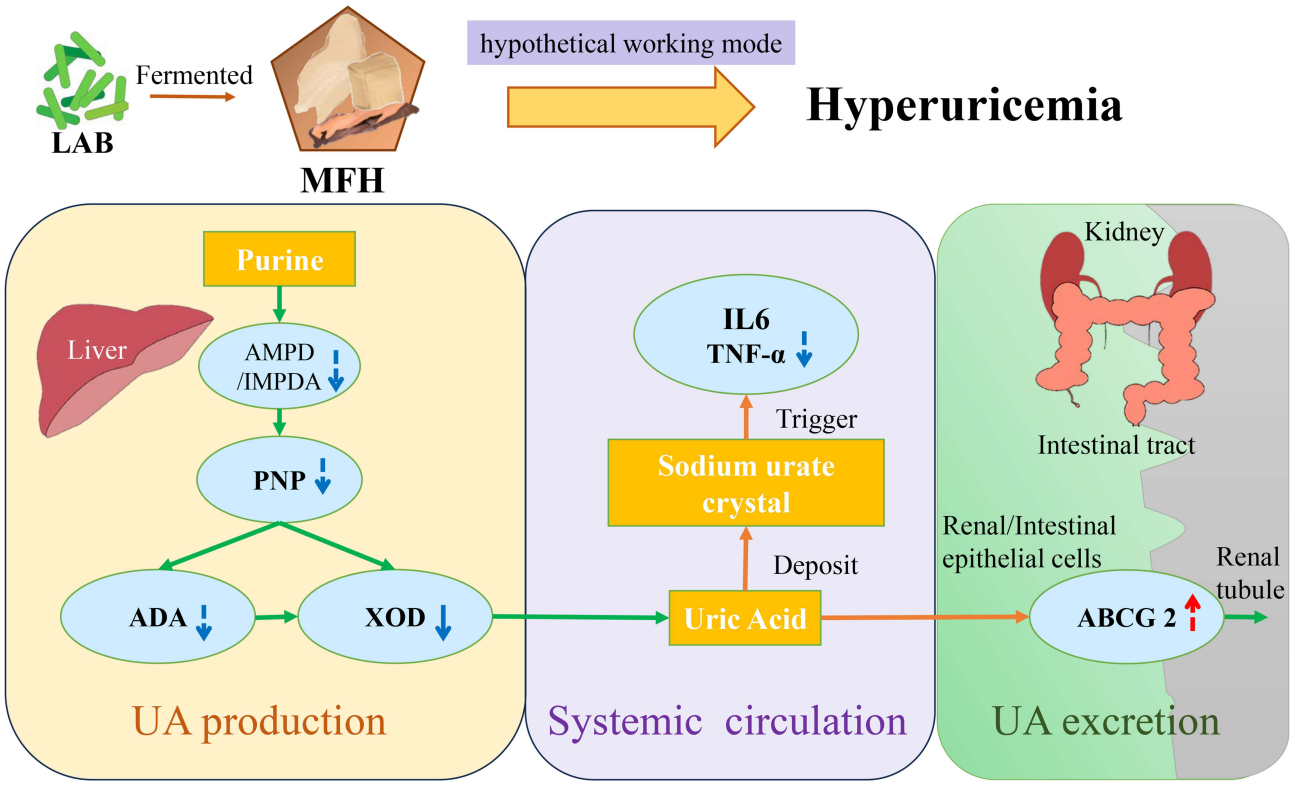

Figure 8 A schematic illustration of the proposed multi-target mechanism of LAB-fermented MFH against hyperuricemia. This diagram presents a hypothetical working model derived from the integrated analysis of metabolomics, network pharmacology, and in vitro assays in this study.
Note: Solid blue arrows illustrate interactions directly verified in this study, while dashed arrows indicate predicted ones. The direction of the arrow signifies the functional effect: upward (↑) for promotion and downward (↓) for inhibition or downregulation.
Abbreviations: MFH stands for medicine and food homology; LAB stands for Lactic Acid Bacteria; XOD stands for Xanthine Oxidase; ADA stands for Adenosine Deaminase; PNP stands for Purine Nucleoside Phosphorylase; AMPD stands for Adenosine Monophosphate Deaminase; IL-6 stands for Interleukin-6; TNF-α stands for Tumor Necrosis Factor-alpha; ABCG2 stands for ATP-binding Cassette Subfamily G Member 2.

Conclusions

This study demonstrates for the first time that *fermented Chaenomeles speciosa (Sweet) Nakai*, *Smilax glabra Roxb*. and *Pueraria montana var. lobata*. alleviate HUA by inhibiting XOD enzyme activity. Metabolomics screening identified 54 significantly upregulated differential metabolites and two key pathways (flavone and flavanol biosynthesis, isoflavone biosynthesis) were identified through metabolomics screening. Combined with network pharmacology analysis, 53 targets, 2 key pathways, and 11 metabolic indicators involved in MFH's intervention on HUA were uncovered. Molecular docking further validated interactions between MFH and these key targets. XOD activity results indicated that LAB fermentation significantly enhanced MFH's inhibitory effect on key enzymes in purine metabolism. This study employed a combined approach of metabolomics detection, network pharmacology, and in vitro enzyme activity validation to preliminarily explore the key targets and mechanisms of action for *Chaenomeles speciosa (Sweet) Nakai*, *Smilax glabra Roxb*. and *Pueraria montana var. lobata*. in treating HUA. This not only enhances the therapeutic efficacy of MFH for HUA but also provides a novel paradigm for further investigating the therapeutic effects of fermenting other medicine and food homology substances using different bacterial strains.

However, it is important to note that the proposed multi-target mechanism is primarily derived from integrated omics predictions and in vitro validation. Thus, future work will focus on assessing the therapeutic potential of FMFH in animal models of hyperuricemia to directly test and refine the proposed multi-target model.

Abbreviations

HUA, Hyperuricemia; MFH, medicine and food homology; FMFH, Fermented medicine and food homology; UA, uric acid; XOD, Xanthine oxidase; LAB, *Lactobacillus*; CS, *Chaenomeles speciosa (Sweet)*; SR, *Smilax glabra Roxb*.; PL,

https://doi.org/10.2147/BTT.S578004

Pueraria montana var. lobate; FCS, fermented *Chaenomeles speciosa (Sweet)*; FSR, fermented *Smilax glabra Roxb.*; FPL, fermented *Pueraria montana var.lobate*.

Data Sharing Statement

Data sharing is not applicable to this article as no datasets were generated or analysed during the current study.

Author Contributions

All authors made a significant contribution to the work reported, whether that is in the conception, study design, execution, acquisition of data, analysis and interpretation, or in all these areas; took part in drafting, revising or critically reviewing the article; gave final approval of the version to be published; have agreed on the journal to which the article has been submitted; and agree to be accountable for all aspects of the work.

Disclosure

The authors declare that they have no competing interests.

References

1. Li S, Zhang B. Traditional Chinese medicine network pharmacology: theory, methodology and application. *Chin J Nat Med*. 2013;11:110–120. doi:10.3724/SP.J.1009.2013.00110
2. Jing Wen Z, Ning W, Hongxia Q, et al. Study on the curative effect of febuxostat on early diabetic nephropathy complicated with hyperuricemia and its influence on patients' renal function. *Shaanxi Med J*. 2020;49(2):209–211.
3. Liu Z, Su X, Xiao M, et al. Association between eating away from home and hyperuricemia: a population-based nationwide cross-sectional study in China. *Biomed Res Int*;2019. 2792681. doi:10.1155/2019/2792681
4. Lanaspa MA, Andres-Hernando A, Kuwabara M. Uric acid and hypertension. *Hypertens Res*. 2020;43:832–834. doi:10.1038/s41440-020-0481-6
5. Xiaoyi S, Mingmia Z, Gang R, et al. Effects of compound Smilax glabra granules on the related physical and chemical indexes and protein levels of hyperuricemia rats with phlegm-dampness constitution. *Chin J Exp Tradit Med Form*. 2016;22(15):100–105.
6. Jing M, Jingzhuo T, Lianying W, et al. Preliminary study on animal model of hyperuricemia suitable for screening traditional Chinese medicine. *Chin J Exp Tradit Med Form*. 2021;27(17):46.
7. Lu Y, Fan -X-X, Zhao S-L, et al. Supplements extracted from *Lophatherum gracile* Brongn. ameliorates hyperuricemia by regulating nucleotide metabolic enzymes and urate transporters. *FMH*. 2025. doi:10.26599/FMH.2026.9420099
8. Wang Y-X, Chen X-L, Zhou K, et al. Fucoidan dose-dependently alleviated hyperuricemia and modulated gut microbiota in mice. *FMH*. 2025. doi:10.26599/FMH.2026.9420095
9. Chinese Pharmacopoeia Commission. *Pharmacopoeia of the People's Republic of China (Part One)*. Beijing: China Medical Science Press; 2020:311.
10. Ruoling X, Peng D, Ma Y, et al. Anti-hyperuricemic effects of extracts from *Chaenomeles speciosa* (Sweet) Nakai Nakai fruits on hyperuricemic rats. *Metabolites*. 2024;14(2):117. doi:10.3390/metabo14020117
11. Fengyang Z, Zhihua X, Guanghuan S, et al. Research progress of treating hyperuricemia with traditional Chinese medicine based on uric acid transporter. *Cent South Pharm*. 2022;20(05):1123–1128.
12. Wu X, Fu S, Jiang M, et al. Sanhuang Xiexin decoction ameliorates DSS-induced colitis in mice by regulating intestinal inflammation, intestinal barrier, and intestinal flora. *J Ethnopharmacol*. 2022;297(115537):115537. doi:10.1016/j.jep.2022.115537
13. Wu H, Wang Y, Huang J, et al. Rutin ameliorates gout via reducing XOD activity, inhibiting ROS production and NLRP3 inflammasome activation in quail. *Biomed Pharmacother*. 2023;158:114175. doi:10.1016/j.biopha.2022.114175
14. Sun Y-J, Cao S-J, Liang F-N, et al. Puerol and pueroside derivatives from Pueraria lobata and their anti-inflammatory activity. *Phytochemistry*. 2023;205:113507. doi:10.1016/j.phytochem.2022.113507
15. Xin Z, Jie C. Research progress of natural active substances with uric-acid-reducing activity. *Agric Food Chem*. 2022;70(50):15647–15664. doi:10.1021/acs.jafc.2c06554
16. Ali A, Zoha M, Soghra M. Scutellaria baicalensis and its constituents baicalin and baicalein as antidotes or protective agents against chemical toxicities: a comprehensive review. *Naunyn Schmiedebergs Arch Pharmacol*. 2022;395(11):1297–1329. doi:10.1007/s00210-022-02258-8
17. Jiadong X, Jiabao Z, Zhiyuan W, et al. Research progress of uric acid excretion and its related transporters in hyperuricemia. *Chin Gen Prac*. 2023;26(15):1916–1922.
18. Liu Z, Guo F, Wang Y, et al. BATMAN-TCM: a bioinformatics analysis tool for molecular mechanism of traditional Chinese medicine. *Sci Rep*. 2016;6:21146. doi:10.1038/srep21146
19. Shang Y-F, Cao H, Ma Y-L, et al. Effect of lactic acid bacteria fermentation on tannins removal in Xuan Mugua fruits. *Food Chem*. 2019;274 (15):118–122. doi:10.1016/j.foodchem.2018.08.120
20. Wang Y-A, Guo X, Zhang M-Q, et al. Evaluation of anti-hyperuricemic and nephroprotective activities and discovery of new XOD inhibitors of Morus alba L. root bark. *J Ethnopharmacol*. 2025;343:119476. doi:10.1016/j.jep.2025.119476
21. Zhuang X-C, Chen G-L, Liu Y, et al. New lignanamides with antioxidant and anti-inflammatory activities screened out and identified from Warburgia ugandensis combining affinity ultrafiltration LC-MS with SOD and XOD Enzymes. *Antioxidants*. 2021;10(3):370. doi:10.3390/antiox10030370

22. Gao P, Chang K, Yuan S, et al. Exploring the mechanism of hepatotoxicity induced by Dictamnus dasycarpus based on network pharmacology, molecular docking and experimental pharmacology. *Molecules*. 2023;28(13):5045. doi:10.3390/molecules28135045
23. Chen M, Zhu J, Kang J, et al. Exploration in the mechanism of action of licorice by network pharmacology. *Molecules*. 2019;24(16):2959. doi:10.3390/molecules24162959
24. Dai G, Liu D, Wang Y, et al. Integrated serum pharmacochemistry and network pharmacology used to explore potential antidepressant mechanisms of the Kaixin San. *Biomed Chromatogr*. 2025;39(4):e70041. doi:10.1002/bmc.70041
25. Zhai Y, Liu L, Zhang F, et al. Network pharmacology: a crucial approach in traditional Chinese medicine research. *Chin J Nat Med*. 2023;21(5):323–332. doi:10.1016/S1875-5364(23)60429-7
26. Li X, Liu Z, Liao J, et al. Network pharmacology approaches for research of Traditional Chinese Medicines. *Chin J Natural Med*. 2023;21(5):323–332. doi:10.1016/s1875-5364(23)60429-7
27. Nguyen H, Pham V-D, Nguyen H, et al. CCPA: cloud-based, self-learning modules for consensus pathway analysis using GO, KEGG and Reactome. *Brief Bioinform*. 2024;25(Supplement_1):bbae222. doi:10.1093/bib/bbae222
28. Nogales C, Mamdouh ZM, List M, et al. Network pharmacology: curing causal mechanisms instead of treating symptoms. *Trends Pharmacol Sci*. 2022;43(2):136–150. doi:10.1016/j.tips.2021.11.004
29. Pan HD, Yao XJ, Wang W-Y, et al. Network pharmacological approach for elucidating the mechanisms of traditional Chinese medicine in treating COVID-19 patients. *Chin J Nat Med*. 2023;21(5):323–332. doi:10.1016/S1875-5364(23)60429-7
30. Peng Y, Zhu G, Ma Y, et al. Network pharmacology–based prediction and pharmacological validation of effects of Astragali Radix on acetaminophen-induced liver injury. *Front Med*. 2022;9. doi:10.3389/fmed.2022.697644
31. Ding Y, Cao ZY, Kezp, et al. Inhibition of rutin against influenza virus in vitro and its mechanism. *Drugs Clin*. 2015;30(12):1431–1436.
32. Cushniee TPT, Lamb AJ . Antimicrobial activity of flavonoids. *Int J Antimicrob Agents*. 2025;26(50):343–356. doi:10.1016/j.ijantimicag.2005.09.002
33. Miao JH, Bai J, Li JC, et al. Effect of rutin on renal function and pathological changes in diabetic nephropathy rats Chin. *J Exp Tradit Med Form*. 2015;21(13):122–125.
34. Rajaram P, Subramanian R. Acute liver failure. *Semin Respir Crit Care Med*. 2018;39:513–522. doi:10.1055/s-0038-1673372
35. Wang D, Li R, Wei S, et al. Metabolomics combined with network pharmacology exploration reveals the modulatory properties of Astragali Radix extract in the treatment of liver fibrosis. *Chin Med*. 2019;14:30. doi:10.1186/s13020-019-0251-z
36. Ru J, Li P, Wang J, et al. TCMSP: a database of systems pharmacology for drug discovery from herbal medicines. *J Cheminform*. 2014;6:13. doi:10.1186/1758-2946-6-13
37. Wang CY, Bai XY, Wang CH, et al. Traditional Chinese medicine: a treasured natural resource of anticancer drug research and development. *Am J Chin Med*. 2014;42:543–559. doi:10.1142/S0192415X14500359
38. Li Y, Shen Z, Zhu B, et al. Demographic, regional and temporal trends of hyperuricemia epidemics in Mainland China from 2000 to 2019: a systematic review and meta-analysis. *Glob Health Action*. 2021;14(1):1874652. doi:10.1080/16549716.2021.1874652
39. Wang X, Wu Q, Liu A, et al. Paracetamol: overdose-induced oxidative stress toxicity, metabolism, and protective effects of various compounds in vivo and in vitro. *Drug Metab Rev*. 2017;49:395–437. doi:10.1080/03602532.2017.1354014
40. Lee WM, Squires RH, Nyberg SL, et al. Acute liver failure: summary of a workshop. *Hepatology*. 2008;47(4):1401–1415. doi:10.1002/hep.22177
41. Tang J, Gao H, Xu Y, et al. The potential of Chinese medicines in the treatment of hyperuricemia. *Am J Transl Res*. 2023;15(4):2291–2303.
42. Liu ZQ, Sun X, Liu ZB, et al. Phytochemicals in traditional Chinese medicine can treat gout by regulating intestinal flora through inactivating NLRP3 and inhibiting XOD activity. *J Pharm Pharmacol*. 2022;74(7):919–929. doi:10.1093/jpp/rgac024
43. Shengnan H, Zhijian L, Bing Z, et al. Analysis of intestinal flora structure of quail with hyperuricemia. *Acta Lab Anim Sci Sin*. 2020;28(1):17.
44. Mohammad CM, Shahidah CA, Fatimah SWMW, et al. Delayed hypersensitivity reaction to allopurinol: a case report. *Malays Fam Physician*. 2023;18:11. doi:10.51866/cr.65
45. Guang Liang C, Liran Z, Sha N, et al. Effects of rhizoma dioscoreae septemlobae saponins on chronic hyperuricemia and expression of uric acid transporter 1 in renal tubules of rats. *Chin J Chin Mater Med*. 2013;38(14):2348–2353.
46. Wang S, Fang Y, Yu X, et al. The flavonoid-rich fraction from rhizomes of Smilax glabra Roxb. ameliorates renal oxidative stress and inflammation in uric acid nephropathy rats through promoting uric acid excretion. *Biomed Pharmacother*. 2019;111:162–168. doi:10.1016/j.biopha.2018.12.050
47. Tang WH, Kitai T, Hazen SL. Gut microbiota in cardiovascular health and disease. *Circ Res*. 2017;120(7):1183. doi:10.1161/CIRCRESAHA.117.309715
48. Xing W, Ning X, Honglei L, et al. Study on the mechanism of Fangji Huangqi Decoction in reducing uric acid and protecting kidney in hyperuricemia mice. *Chin J Chin Mater Med*. 2020;45(21):5248.